JOURNAL OF SPACECRAFT AND ROCKETS
Vol. 35, No. 4, July–August 1998

New Three-Dimensional Inverse Method for High-Speed Vehicle Design

Jae Woo Lee*
Kon-Kuk University, Seoul 143-701, Republic of Korea
and
W. H. Mason†
Virginia Polytechnic Institute and State University, Blacksburg, Virginia 24061

An inverse design method for fully three-dimensional supersonic and hypersonic bodies was developed for computer codes based on the Euler equations. The method is designed to be easily incorporated into existing analysis codes. The aim of the method is to provide the aerodynamic designer with a powerful tool for design of aerodynamic shapes of arbitrary cross section. Convergence acceleration techniques were developed and applied successfully to three-dimensional test cases. A three-dimensional body geometry modification method was developed with a new concept for the three-dimensional body slope angle. Examples are presented applying the method to a nonaxisymmetric fuselage-type pressure distribution and a cambered wing-type application. The method performs equally well for both nonlifting and lifting cases.

Nomenclature

$A(M_L, \theta)$	= coefficient of surface pressure-body shape rule; Eqs. (10) and (12)
a	= major axis length
b	= minor axis length
C_p	= pressure coefficient
C_p^T	= target pressure coefficient at the body surface
c	= coefficient defined by Eq. (13)
i	= marching plane index
$j\dim$	= number of grid points along the circumferential direction
k	= inverse iteration count
l	= total body length
M_L	= local Mach number at the body surface
M_∞	= freestream Mach number
$\boldsymbol{n}$	= unit normal vector in each grid cell
P	= slope of the line between points B and C; Eq. (20)
R	= body radius
s	= circumferential distance
u, v, w	= velocity components in x, y, and z directions at the body surface
V_∞	= freestream velocity
x, y, z	= physical coordinates
$y_{\max}$	= maximum value of y at the end of a body
α	= angle of attack
γ	= ratio of specific heats
δ_1, δ_2	= convergence criteria for the inverse calculation
$\theta_{\boldsymbol{n}}$	= body slope angle between surface normal vector and freestream
θ_0	= body slope angle obtained from the surface streamline
θ_1	= corrected body slope angle
τ	= constant; Eq. (14)
ϕ	= circumferential angle

Introduction

AERODYNAMIC analysis methods have progressed very rapidly with the development of computational fluid dynamics (CFD). With renewed interest in design concepts for application to the high-speed civil transport or space launchers as new-generation vehicles,[1] practical aerodynamic design methods in the supersonic- and moderated-hypersonic-speed range are required. However, design methods have not received the same level of attention that analysis methods have received. The need for inverse methods has been cited as a pacing item in at least one advanced supersonic technology study.[2]

Candidate aerodynamic design methods are generally divided into two categories: inverse methods and numerical optimization using direct analysis methods. These two design methods are contrasted in Ref. 3.

Although numerous inverse design methods have been developed previously, most of them are directed toward wing design at transonic speeds.[4,5] Less effort has been devoted to the development of inverse methods for supersonic and hypersonic bodies.[6] This is especially true for arbitrary three-dimensional bodies. Furthermore, an important consideration in supersonic/hypersonic design is the use of methods that exploit the space-marching techniques available for high-speed flow. Finally, the issue of determining the planform shape as well as body contours within a specified planform outline, which is the usual case with transonic/subsonic inverse methods, must be considered.

A new inverse method, which accounts fully for three-dimensional flowfields and body shapes for supersonic and hypersonic bodies, is developed. This inverse method is intended to be a method that can be readily incorporated into existing analysis codes. Considerable effort is devoted to the development of a method demonstrating rapid convergence due to the large computational times required in three-dimensional flowfield analysis. Convergence acceleration techniques are proposed and demonstrated, and the method is applied to two three-dimensional body test cases at angle of attack.

Description of the Method

The three-dimensional inverse method is an extension of a method for axisymmetric bodies.[6] The method is specifically designed for conditions when space marching is valid, namely, supersonic/hypersonic flow with no recirculation. The geometry at each downstream station x is determined before proceeding to the next station; an iterative procedure is followed at each station. One initial plane of data, including pressure and geometry, is required to start the calculation. To develop an inverse method in three dimensions, the following key factors of the procedure must be considered.

1) A grid point for the kth iteration at a specified station is not a grid point for the $k+1$st iteration. Both y and z components of each grid point in the crossflow plane change during the inverse iterations,

Received Feb. 1, 1998; accepted for publication April 15, 1998.

*Assistant Professor, Department of Aerospace Engineering. Member AIAA.
†Professor, Department of Aerospace and Ocean Engineering. Associate Fellow AIAA.

and numerical interpolation and curve fitting are inevitably required. The interpolation procedures must be robust. The specification of the target pressure distribution requires special consideration.

2) The body slope angle and its sign (positive or negative), which can be clearly defined in the two-dimensional or axisymmetric case, should be newly defined because the slope of the surface streamline cannot be described by only one body slope angle.

General Approach

Two approaches for the three-dimensional inverse method can be considered: One corrects the body geometry on the axial surface grid line and the other on the surface streamline. In two-dimensional or axisymmetric flow, there is no difference between the axial grid line and the streamline at the surface. In general, these two are different for three-dimensional flow.

In the approach using the grid line, the new surface grids are obtained directly from the inverse procedure; numerical interpolation and curve fitting are not necessary. In three dimensions, there is no obvious physical basis for the surface geometry correction along a grid line, and thus this approach is not appropriate.

In the streamline approach, surface geometry is adjusted along the surface streamline by applying a two-dimensional pressure-shape rule along the streamline to obtain the actual three-dimensional body modification. This provides a rational basis for adjustment of the shape to attain a specified pressure distribution. Davis[7] also used this approach for supersonic conical flow. In this approach, numerical interpolation and curve fitting are needed for each inverse iteration because the coordinates of the modified body are not the grid points. Inasmuch as the surface pressure-body shape rules,[6] which will be discussed in detail in the next section, are derived based on two-dimensional theory, application of the rules along surface streamlines is the most physically appropriate method of modifying the three-dimensional body geometry with a two-dimensional surface pressure-body shape rule.

The present method will be applied using the Euler equations to describe the flowfield. The streamline approach for the modification of the body geometry is selected and developed because of its physical basis. One consequence of a three-dimensional method is that the planform semispan $y_{\max}$ is obtained during the inverse iteration rather than given as an input. If it is fixed or given as an input, the problem statement is not fully three dimensional in a strict sense. Using this iterative method, the initial estimate for the body shape at the station where the pressure is specified can be arbitrary, and different initial body shapes will be used here to demonstrate the method. However, to accelerate the convergence, it is better to define an initial body shape using the surface pressure-body geometry relations and the solution at the previous plane.

Because the planform shape changes during the inverse iterations, the method of specifying the target pressure distribution is not obvious. Several possibilities can be considered. The circumferential angle ϕ, circumferential distance s, or the y (spanwise) coordinate could be used. The first two methods are not appropriate in the present inverse procedure because of the difficulty of defining the points in the crossplane. The third method is the most applicable approach. The target pressure will be given by y coordinates nondimensionalized by the semispan length in each crossflow plane. That means the target pressure locations change as the body shape changes. In comparison to the two-dimensional case, the question of scale arises, and the specification of a pressure distribution is more complicated in the three-dimensional case.

Two convergence criteria are introduced. One is the tolerance for maximum difference of the pressure coefficient to the target C_p across the crossflow plane, and the other is the total grid point average of root mean square of the same difference:

$$\Delta C_{p\max} = \text{maximum of } \left|C_p^T - C_{p_j}\right| \quad \text{for} \quad j = 1, j\dim - 1 \tag{1}$$

$$\Delta C_p 2 = \frac{\sqrt{\sum \left(C_p^T - C_{p_j}\right)^2}}{j\dim - 1} \tag{2}$$

The typical values of these criteria are $\Delta C_{p\max} < \delta_1 = 0.001$ and $\Delta C_p 2 < \delta_2 = 0.0005$.

The inverse procedure starts with a given freestream Mach number, initial body shape and pressure distribution at an upstream data plane, and specified target pressures at downstream stations. The method steps one grid plane at a time, using the same approach at each crossflow plane station. At each station, an initial estimate i is made for the geometry, and the surface pressure distribution is obtained from an Euler code. Using the difference between the pressures obtained for the current iteration geometry and target pressure distribution, updated body geometry at the ith marching plane is obtained. The details for the process are included in the three-dimensional inverse procedure explanation in the next section. The process is repeated until convergence is achieved.

Detailed Methodology

The three-dimensional inverse method begins by adjusting the surface geometry in the plane of the surface streamline, which is the plane defined by points A, B, and C in Figs. 1a and 1b. Point A is a cell-centered point between the first and the ith crossflow plane, which is known a priori. Point B is a point located in the ith crossflow plane, which has the same y and z coordinates as point A. Point C is obtained from the surface streamline vector and point B. The body surface slope angle is also obtained from the surface streamline. Using the surface pressure-body geometry rule,[6] an updated body geometry (point D) is obtained. D_P and D_M in Figs. 1a and 1b denote geometry point D with positive and negative θ_1, respectively. Finally, the new grid points are generated from the updated body geometry using numerical interpolation and curve fitting. The details of each step are given as follows.

Definition of θ_0

The slope angle θ of the three-dimensional body is usually defined as the angle between the surface normal vector and freestream velocity vector:

$$\sin\theta_a = \frac{\boldsymbol{V}_\infty}{|\boldsymbol{V}_\infty|} \cdot \hat{\boldsymbol{n}} \tag{3}$$

However, this definition of θ is not adequate for the present inverse procedure. The body shape is modified on the surface streamline, which cannot be uniquely determined by θ_a alone. Thus, the body slope angle θ must be defined in a different way. In the new inverse method, θ is defined as the angle between the streamline and the x

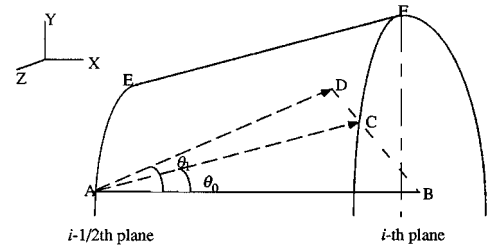

a) Overall orientation

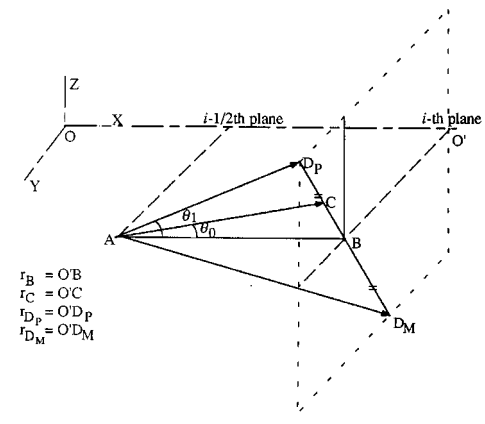

b) Detailed point definition

Fig. 1 Body geometry correction along the surface streamline.

axis. This angle is used for body modification, whereas θ_a is used to calculate $A(M_L, \theta)$, which is an approximate relation between changes in pressure and changes in slope along the streamline (as investigated in Ref. 6). Because $A(M_L, \theta_a)$ is derived from the local inclination method, $A(M_L, \theta_a)$ is defined by the equation

$$\Delta C_p = A(M_L, \theta_a)\Delta\theta \tag{4}$$

For the zero-angle-of-attack case, there is typically only a small difference between θ and θ_a, and the converged body geometry can be obtained using only θ. For the nonzero-angle-of-attack case, the effect of θ_a is large, and a converged body geometry will not be obtained without considering θ_a. The body slope angle θ is expressed by the surface velocity vector

$$\theta_{0_j} = \cos^{-1}\left[\frac{u_j}{\left(u_j^2 + v_j^2 + w_j^2\right)^{\frac{1}{2}}}\right] \tag{5}$$

Next consider y_C and z_C (y and z coordinates of the point C in Figs. 1a and 1b). AC is the surface streamline that passes through point A and is known. C is the intersection point of the surface streamline to the crossflow plane of the ith station. The values of y_C and z_C can be easily determined using surface velocity components u_j, v_j, and w_j from

$$y_{C_j} = y_B + (\Delta x/2)\cdot(v_j/u_j) \tag{6}$$

$$z_{C_j} = z_B + (\Delta x/2)\cdot(w_j/u_j) \tag{7}$$

Sign of θ_0

As can be seen in Eq. (5), the sign of θ_0 is not known. The sign is found by considering the length from the point O′ as shown in Fig. 1b, i.e.,

$$\theta_{0_j} = \theta_{0_j} \qquad \text{for} \qquad r_C \geq r_B \tag{8}$$

$$\theta_{0_j} = -\theta_{0_j} \qquad \text{for} \qquad r_C < r_B \tag{9}$$

where r_B and r_C are the distances from the x axis to points B and C, respectively. This procedure is needed to apply local two-dimensional theory along a streamline in the three-dimensional case.

$A(M_L, \theta_a)$ and θ_1

Here θ_1 is obtained by the surface pressure-body geometry rule, which was investigated by the authors in a previous paper.[6] Two surface pressure-body geometry rules that have good convergence behavior[6] are selected: the shock-expansion rule and the tangent-cone rule.

With the shock-expansion pressure-shape rule,

$$A(M_L, \theta_a) = m\cos\theta\cdot\left[(2/M_L) + (\gamma+1)m\sin\theta_a + \tfrac{3}{16}(\gamma+1)^2 m\sin^2\theta_a\right] \tag{10}$$

where

$$m^2 = \frac{M_L^2}{M_L^2 - 1} \tag{11}$$

With the tangent cone pressure-shape rule,

$$A(M_L, \theta_a) = \tau\left(2\theta_a + \tfrac{1}{2}c\theta_a^{-\frac{1}{2}}\right) \tag{12}$$

where

$$c = \left(5\gamma M_L^{\frac{3}{2}}\right)^{-1} \tag{13}$$

and

$$\tau = \frac{2(\gamma+1)(\gamma+7)}{(\gamma+3)^2} \tag{14}$$

For each body point, θ_1 can be calculated from

$$\theta_{1_j} = \theta_{0_j} + \frac{C_p^T - C_{p_j}}{A(M_L, \theta_a)} \tag{15}$$

Because the tangent-cone rule is not applicable for negative body slope regions,[6] the shock-expansion rule is selected; it is valid for all body slopes.

Corrected Body Geometry (y_D, z_D)

Coordinates y_D and z_D (y and z coordinates of the point D in Figs. 1a and 1b) are the corrected surface geometry by the new surface slope angle θ_1. In Figs. 1a and 1b, the points B, C, and D lie on the same line, and line AB is perpendicular to line BD. Therefore, the coordinates y_D and z_D are obtained by

$$y_{D_j} = y_{B_j} + \mathrm{d}y_{D_j} \tag{16}$$

$$z_{D_j} = z_{B_j} + \mathrm{d}z_{D_j} \tag{17}$$

where

$$\mathrm{d}y_{D_j} = \pm\frac{\tan\theta_{1_j}}{\sqrt{\left(1 + P_j^2\right)}}\cdot\frac{\Delta x}{2} \tag{18}$$

$$\mathrm{d}y_{D_j} = P_j\cdot\mathrm{d}y_{D_j} \tag{19}$$

with

$$P_j = \frac{z_{C_j} - z_{B_j}}{y_{C_j} - y_{B_j}} \tag{20}$$

To select only one value (y and z coordinates) from Eqs. (16) and (17), the distances from the x axis are calculated for points B, C, D_P, and D_M. These distances are denoted by r_B, r_C, r_{D_P}, and r_{D_M}, respectively. By comparing r_{D_P} and r_{D_M} with r_B and by considering the sign of θ_1, D_P or D_M is selected as a new body point. Specifically, D_P is selected as a new body point D when r_{D_P} is greater than r_B and the sign of θ_1 is positive; D_M is selected when r_{D_P} is smaller than r_B and the sign of θ_1 is positive. For the negative value of θ_1, D_P is selected as a new body point D when r_{D_P} is smaller than r_B. D_M is selected when r_{D_P} is greater than r_B. The rationale of this selection procedure is based on the three-dimensional concept of body slope angle. The procedure is repeated until the difference between the target pressure and the pressure at iteration level k satisfies the convergence criteria.

Methods of Accelerating the Convergence

The converged body shape can be obtained reliably using the procedure just described. Typically, at least 10 inverse iterations are required for the test cases presented in the next section. Thus, an improvement in the convergence behavior is desired inasmuch as rapid convergence is an important consideration in developing a practical method. Four convergence acceleration methods are considered.

Reduced Grid Density

Although the number of grid points at each crossflow plane should be large enough to obtain an accurate body shape with any distribution of the interpolation input points, consideration was given to reducing the grid density. (Dense three-dimensional grid calculations usually require large computational times.) Crossflow plane grids of 41 × 30 and 31 × 20 are examined in the next section.

Unconverged Intermediate Design Solutions

The usual convergence criterion adopted for CFD analysis is a four-order-of-magnitudedecrease in the residual. This takes a large computational time, especially for the last order-of-magnitude decrease of the residual. Thus, it is proposed to use a convergence criterion that is not as strict, namely, a two-and-one-half-order-of-magnitude decrease in residual. In other words, solutions (velocities, pressures, and local Mach numbers) that were not fully converged are used to begin the next inverse iteration. The starting residual values decrease as the inverse iterations progress. Thus, the present convergence criterion provides quite accurate results in the final inverse iteration and in addition reduces the computational time. This approach results in an approximately threefold decrease in time to obtain a design solution.

Regula-Falsi Root-Finding Scheme

In Ref. 6, the inverse problem was considered as a root-finding problem, where the root is the geometry that produces a zero difference between the target C_p and the C_p produced by the body shape. By applying the regula-falsi root-finding scheme to the axisymmetric inverse problems, the convergence behavior was dramatically improved. Therefore, the regula-falsi scheme is introduced again and demonstrated for the three-dimensional example calculations. This method resulted in approximately 1.5–5 times faster convergence.

Iteration in Real Sense

Because the surface pressure-body geometry rule is derived for zero angle of attack, a modification to the method is needed to accelerate the convergence when the effect of angle of attack is considered. In the normal operation of the method, θ_0 at the $k+1$st iteration level is obtained from the updated body geometry, not from θ_1 at the kth iteration level. To accelerate convergence, replace $\theta_1^{(k)}$ with $\theta_0^{(k+1)}$ when $\Delta C_p 2$ is relatively small (typically $\Delta C_p 2 < 0.005$).

Using these four convergence acceleration techniques, the convergence is 10–20 times faster than the basic method, resulting in very significant savings in computational time. Each of these convergence acceleration methods is applied to the test cases and is discussed in detail in the next section.

Results and Discussion

The new three-dimensional inverse procedure that was just developed and explained is now applied to test cases in the supersonic ($M_\infty = 3.0$) and hypersonic ($M_\infty = 6.28$) flow regimes. Two body geometries, an elliptic cone and a winglike nonconical cambered body, are considered at various angles of attack. The test cases were computed using the computer code CFL3DE.[8] Grids of 41×30 and 31×20 crossflow plane points (circumferential and radial distributions, respectively) were selected based on previous work.[9] (Grid density convergence was studied for power-law bodies over a wide Mach number range in Ref. 9.) Typical computational time for one crossflow plane calculation of both test cases was 5–6 min for the 41×30 grid and 2–3 min for the 31×20 grid system on an IBM 3090 computer.

Using the relatively simple body geometry (elliptic cone) to establish a target pressure distribution, several numerical experiments were performed. Using the information from these numerical experiments, the method was finalized.

1) The convergence acceleration techniques that were proposed in the preceding section (reducing the grid density, using unconverged intermediate solutions, applying the regula-falsi root-finding scheme, and iteration in real sense) were applied and tested one by one.

2) By considering several different initial body geometries for the same target pressure distribution, the capability of the method to find the planform shape and the exact body geometry was proven.

3) The effect of different surface pressure-body geometry rules was investigated.

4) The capability of the method to find the exact geometry for a body with angle of attack of $\alpha = 10$ deg is demonstrated.

5) From the example calculation of the winglike nonconical cambered body, the capability of the method to find the body geometry that has a rapid pressure variation across the crossflow plane was investigated.

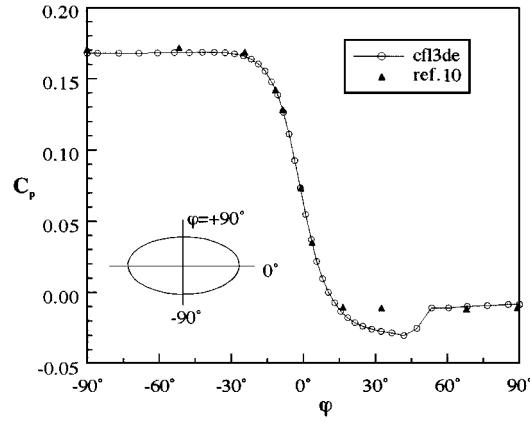

Fig. 2 Comparison of surface pressure coefficient with experimental data for the elliptic cone test case: $M_\infty = 5.8$ and $\alpha = 10$ deg.

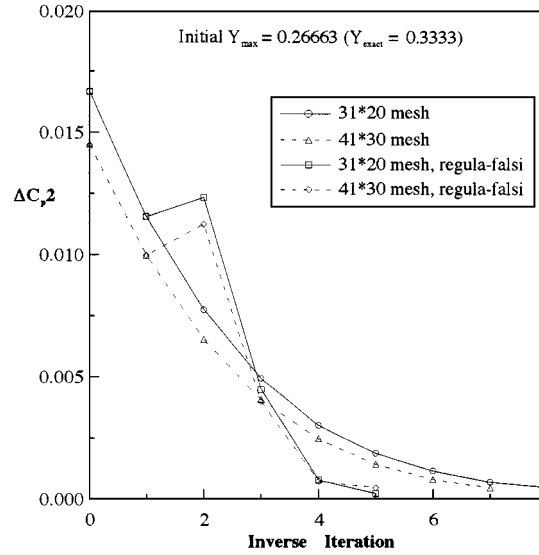

Fig. 3 Convergence behavior of the elliptic cone test case for different grid densities and regula-falsi option; initial $y_{max} = 0.26663$, $M_\infty = 6.28$, and $\alpha = 0$ deg.

Before making inverse calculations, the present application of the basic analysis code was validated by making computation and comparing the results with previously obtained results. The calculation was performed for an elliptic cone (ratio of major axis length to minor axis length $a/b = 2.0$) at $M_\infty = 5.8$ and $\alpha = 10$ deg. As shown in Fig. 2, the pressure coefficients at the body surface are in good agreement with the experimental results,[10] except in the region of separation ($15 < \phi < 50$ deg). This experimental case was previously used by Siclari and Rubel[11] to validate a computational technique for correcting potential flow solutions, and identical results were obtained. Having verified the basic accuracy of this analysis code, the inverse calculations were undertaken.

Elliptic Cone Test Case

The elliptic cone is a simple nonaxisymmetric body shape, which is a good candidate for evaluation of the method. To test the method, the pressure distribution obtained from an analysis calculation of the known body geometry is specified as a target pressure distribution, and an arbitrary body geometry is used as an initial body shape.

The convergence acceleration techniques already discussed were tested for different initial body geometries ($y_{max,\,initial} = 0.26663$ and 0.4) at $M_\infty = 6.28$ and $\alpha = 0$ deg. Results are shown in Fig. 3, where the effects of grid density and the regula-falsi scheme are investigated for the $y_{max,\,initial} = 0.26663$ case. Only a small improvement in convergence was obtained using the higher grid density.

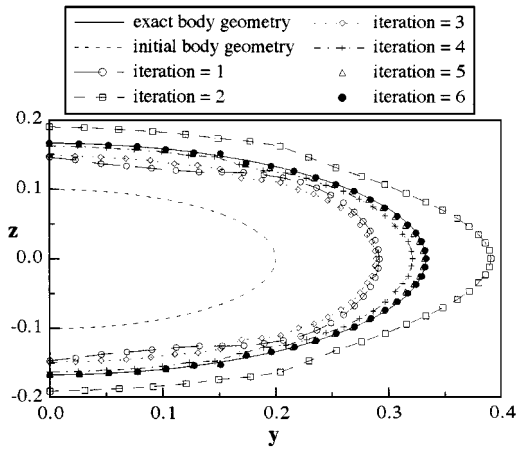

Fig. 4 Body geometry convergence of the elliptic cone test case: M_∞ = 6.28 and α = 0 deg.

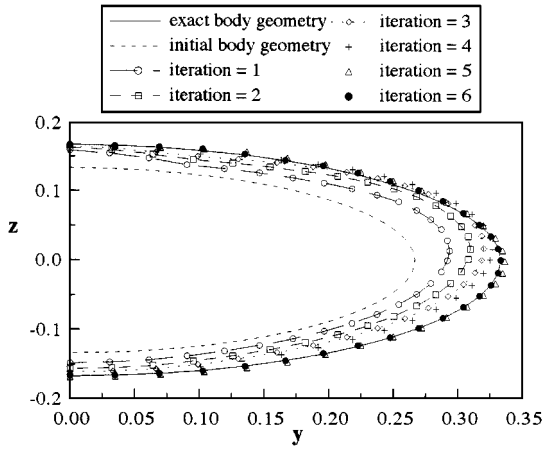

Fig. 5 Body geometry convergence of the elliptic cone test case: M_∞ = 6.28 and α = 10 deg.

The advantages of the regula-falsi scheme are clearly shown. As two normal operations of the inverse method were needed to start the regula-falsi scheme, $\Delta C_p 2$ at the first two inverse calculations with and without regula-falsi scheme are the same. Then the regula-falsi method takes effect, and $\Delta C_p 2$ decreases rapidly as the iterations progress. It took only four to five inverse iterations to obtain a converged body geometry using regula-falsi. Even with the normal operation of the method, the converged body geometry was obtained within 10 inverse iterations. More than a factor of 10 savings in computation time can be obtained by using these techniques. The convergence of the body geometry for each inverse iteration is shown in Fig. 4 for the case using an initial $y_{max} = 0.2$. During the iteration the body geometry changed arbitrarily and converged to the exact body geometry within six inverse iterations. From Figs. 3 and 4 it is seen that the method works well: The initial body geometry can be specified nearly arbitrarily, and the convergence acceleration techniques also work.

The possible complications due to angle of attack were considered for the elliptic cone at $M_\infty = 6.28$. Body geometry and C_p convergence behavior are shown in Figs. 5 and 6. The convergence acceleration techniques (including the use of iteration in real sense) were also applied for this inverse calculation. The results show that, even with the presence of a pressure peak, the converged body geometry was found within about six iterations.

For several initial body geometries ($y_{max} = 0.2$, 0.26663, and 0.4), the present inverse method is also applied at supersonic speed ($M_\infty = 3.0$) with and without the regula-falsi scheme. The results are shown in Fig. 7 for the case with initial $y_{max} = 0.4$. Converged body geometries were obtained within six to eight iterations without the regula-falsi scheme and four to six iterations using the regula-falsi scheme.

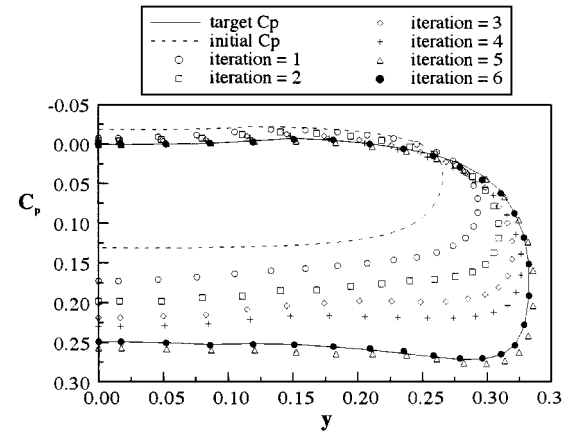

Fig. 6 Pressure coefficient convergence of the elliptic cone test case: M_∞ = 6.28 and α = 10 deg.

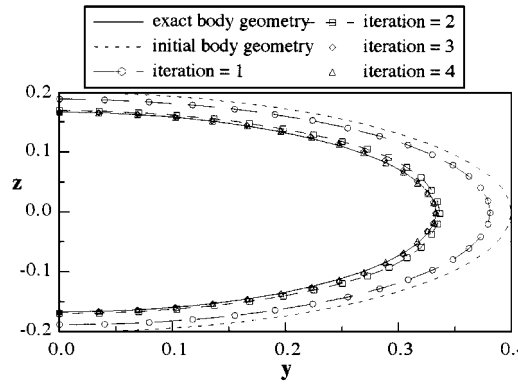

Fig. 7 Body geometry convergence of the elliptic cone test case: M_∞ = 3.0 and α = 0 deg.

Winglike Nonconical Cambered Body

Another case was selected to evaluate the method for cases with larger variation in pressure around the leading edge. The nonconical cambered body is a relatively simple three-dimensional body, but it has a rapid decrease in surface pressure near the attachment line as the flow expands around the edge. Thus, this body geometry is a good test case for the three-dimensional inverse procedure development and provides a demonstration of its robustness. Conically cambered shapes at supersonic speed were investigated in detail in Ref. 12.

To reduce the computation time, $\frac{3}{4}$ of the body length from the nose was taken to be an elliptic cone shape. The remaining portion of the body was a nonconical $\frac{3}{4}$-power-law shape. The cross-sectional body geometry in each marching plane was determined by the camber angle at the y_{max} point, the base elliptic cone ($a/b = 3$), and the $\frac{3}{4}$-power-law shape along the x axis. The camber angle varies from 0 deg (elliptic cone) at $x/l = 0.75$ to -12 deg at $x/l = 1.0$, with a cosine curve to define the spanwise camber. The computational grid and the cross-sectional body shape at $x/l = 1.0$ (camber angle $= -12$ deg) are shown in Fig. 8. To resolve the sharp decrease in the pressure near y_{max}, 41 crossflow plane grid points in the circumferential direction were used. Six stations were constructed for the nonconical axial portion of the body, and the present inverse procedure was applied only to the last station.

Each convergence-acceleration technique was applied to this test case. The body geometry convergence at zero angle of attack is shown in Fig. 9. The converged body shape was obtained within eight iterations and correctly reproduced the target pressure distribution. There was no significant difference in convergence behavior between the case using the regula-falsi scheme and the case without it. The convergence history looked slightly better in the case with regula-falsi, but there is no difference in the number of iterations required to obtain convergence.

Results for 10-deg angle of attack are shown in Figs. 10, 11a, and 11b. The number of iterations to obtain a converged body geometry

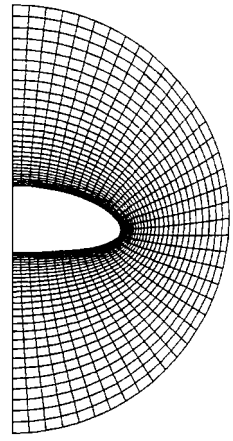

Fig. 8 Crossflow plane computational grid for cambered body at x/l = 1.0.

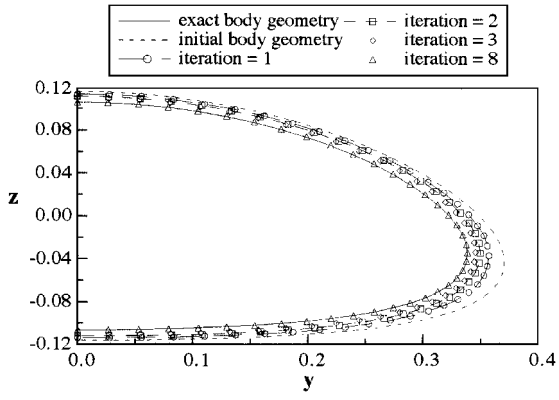

Fig. 9 Body geometry convergence of the cambered body: M_∞ = 6.28 and α = 0 deg.

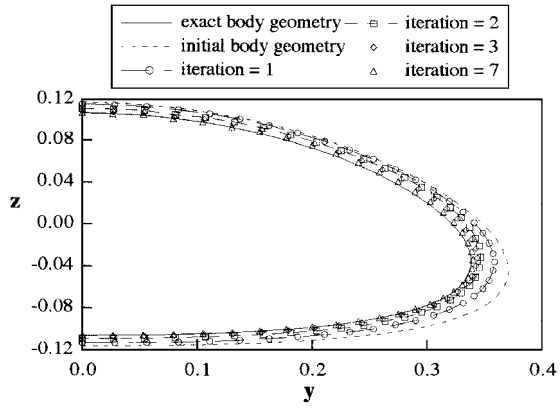

Fig. 10 Body geometry convergence of the cambered body: M_∞ = 6.28 and α = 10 deg.

was slightly higher than that of the zero-angle-of-attack case (nine inverse iterations). The convergence history for the body shape is shown in Fig. 10. The pressure distribution convergence histories are presented in Figs. 11a and 11b. Note that the sharp decrease in pressure near y_{max} was correctly reproduced as the iteration proceeded. The $\alpha = 10$ deg case showed that the method had no problem in finding the body shape on the upper surface, when the pressure coefficients were negative over the entire region. The convergence behavior for computations including angle-of-attack effects had nearly the same trend as that for the zero-angle-of-attack case.

The overall computation time depends on the initial estimate of the body geometry, freestream Mach number, and the inverse calculation options (regula-falsi, etc.). Typical computational times required to obtain the body geometry in one crossflow plane were approximately twice the time required to obtain a similar result without inverse design iterations.

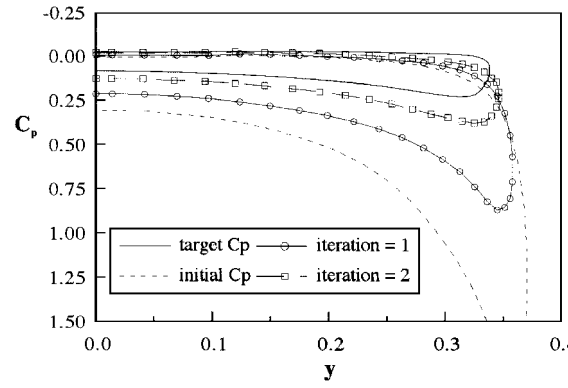

a) Inverse iterations 0–2

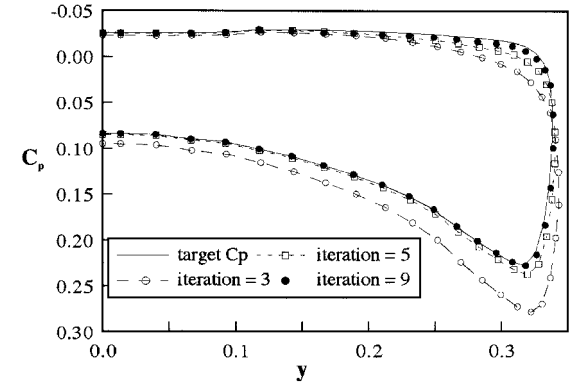

b) Inverse iterations 3–9

Fig. 11 Pressure coefficient convergence of the cambered body: M_∞ = 6.28 and α = 10 deg.

Conclusions

A new inverse method has been presented for three-dimensional body design in the supersonic and hypersonic flow regimes. A new approach of modifying the body geometry along the surface streamline was developed with a new concept for the body slope angle. Techniques to accelerate the convergence during the inverse iterations were proposed and run successfully for three-dimensional test cases. Example calculations were presented for three-dimensional test cases with angle of attack to demonstrate the robustness of the method in both supersonic and hypersonic flow regimes.

This new method is robust and useful for the aerodynamic design of three-dimensional bodies in the supersonic-to-moderate-hypersonic flow regimes. Further study will be focused on the extension of the current method to viscous flow for which the parabolized Navier–Stokes equations are valid.

Acknowledgment

We would like to acknowledge R. W. Walters for providing us with access to CFL3DE and consulting with us on the use of the code for this work.

References

[1] Scott, W. B., Dornheim, M. A., Smith, B. A., and Ott, J., "The Future of High-Speed Flight," *Aviation Week and Space Technology*, Oct. 1997, pp. 62–76.

[2] Powell, A. G., Agrawal, S., and Lacey, T. R., "Feasibility and Benefits of Laminar Flow Control in Supersonic Cruise Airplanes," NASA CR-181817, July 1989.

[3] Lee, J. W., "Efficient Inverse Methods for Supersonic and Hypersonic Body Design, with Low Wave Drag Analysis," Ph.D. Thesis, Dept. of Aerospace and Ocean Engineering, Virginia Polytechnic Inst. and State Univ., Blacksburg, VA, April 1991.

[4] Volpe, G., and Melnik, R. E., "The Role of Constraints in the Inverse Design Problem for Transonic Airfoils," AIAA Paper 81-1233, June 1981.

[5] Weed, R. A., Anderson, W. K., and Carlson, L. A., "A Direct-Inverse Three-Dimensional Transonic Wing Design Method for Vector Computers," AIAA Paper 84-2156, Aug. 1984.

[6]Lee, J. W., and Mason, W. H., "Development of an Efficient Inverse Method for Supersonic and Hypersonic Body Design," *Journal of Spacecraft and Rockets*, Vol. 31, No. 3, 1994, pp. 400–405.

[7]Davis, W. H., Jr., "Technique for Developing Design Tools from the Analysis Methods of Computational Aerodynamics," *AIAA Journal*, Vol. 18, No. 9, 1980, pp. 1080–1087.

[8]Thomas, J. L., van Leer, B., and Walters, R. W., "Implicit Flux-Split Schemes for the Euler Equations," AIAA Paper 85-1680, July 1985.

[9]Mason, W. H., and Lee, J. W., "On Optimal Supersonic/Hypersonic Bodies," AIAA Paper 90-3072, Aug. 1990.

[10]Chapkis, R. L., "Hypersonic Flow Over an Elliptic Cone: Theory and Experiment," *Journal of the Aeronautical Sciences*, Vol. 28, 1961, pp. 844–864.

[11]Siclari, M. J., and Rubel, A., "Entropy Corrections to Supersonic Conical Nonlinear Potential Flows," *Computers and Fluids*, Vol. 13, No. 3, 1985, pp. 337–359.

[12]Mason, W. H., "SC^3—A Wing Concept for Supersonic Maneuvering," AIAA Paper 83-1858, July 1983.

R. M. Cummings
Associate Editor